4-2008

Modeling and Characterization of Adaptive Lanthanum-Modified Lead Zirconate Titanate (PLZT) Microlenses

Yasser A. Abdelaziez
University of Dayton

Partha P. Banerjee
University of Dayton, pbanerjee1@udayton.edu

eCommons Citation

Modeling and characterization of adaptive lanthanum-modified lead zirconate titanate (PLZT) microlenses

Yasser A. Abdelaziez[*]
Partha P. Banerjee
University of Dayton
Department of Electrical and Computer
   Engineering and Electro-Optics
Dayton, Ohio 45469

Abstract. We report the modeling and characterization of adaptive voltage controlled electro-optic microlenses. First, we utilize finite element analysis (FEA) to simulate the induced electro-optic effect in lanthanum-modified lead zirconate titanate (PLZT). FEA simulation provides microlens parameters such as phase and focal length. A simple z-scan method is developed to fully characterize the adaptive voltage controlled linear lens. Experimental z-scan results are shown to match the theoretical predictions from FEA. © *2008 Society of Photo-Optical Instrumentation Engineers.* [DOI: 10.1117/1.2894795]

1 Introduction

Over the past two decades, semiconductor miniaturization technologies have advanced rapidly, with dimensions becoming comparable to the wavelength of light.[1] Parallel to that, micro-electro-mechanical systems (MEMS),[2] which are based on such technologies, have been evolving strongly, adding a new dimension of complexity and functionality that emulates its founding technology—namely, VLSI. Device miniaturization and integration to achieve microsystems for different applications has introduced new ideas and techniques to produce such devices. Today, the field of MEMS has been split, based on applications, into MOEMS,[3,4] Bio-MEMS,[5] and NMEMS,[6] which stand for optical, biological, and nano applications, respectively, with sub titles such as biophotonics[7] as a subset of Bio-MEMS and MOEMS. For MEMS, as an enabling technology, the objectives will always drive the technology.

Micro-optics technology, MOEMS, is an area of research that addresses a variety of applications. As wide and diverse as the MEMS field itself, micro-optics serves the telecommunication,[8] display,[9] biosensor,[10] optical detection,[11] and imaging[12] industries. Furthermore, microlens arrays[13] are used in lithography,[14] array generation,[15] interconnect,[16] laser beam steering,[17] and shaping[18] applications.

Laser beam shaping (LBS) can be defined as the art of controlling the amplitude and phase of the beam.[19] The benefit of controlling laser beam shape can be seen in improving the uniformity and brightness for imaging, interferometry, lithography, material processing, and optical information and image processing. By splitting and controlling the optical beam wave front amplitude and phase, one can accomplish beam shaping. Computer-generated holograms,[20] polarization effects,[21] and refractive optics[22] have been utilized for such purposes. More recently, microlens arrays have played a crucial rule in beam shaping technique development.[23] Utilizing adaptive optics techniques in beam shaping applications not only gives better control over the desired beam shape, but it also allows for building more modular systems, which have been proposed earlier.[24]

The ability to alter the focal length of a microlens within an array offers the opportunity to track a moving object or to steer optical channels, thereby attracting a significant amount of interest, particularly from the optical computing community. This class of microlenses can be divided into categories based on the material and operation principle used. Electrically tunable microlenses utilize the electro-optic (EO) properties of liquid crystals (LC)[25,26] and ferroelectric (FE) materials such as $LiTaO_3$.[27] In addition, an electrically tunable microlens using liquid bubbles has been demonstrated.[28] More recently, hydrodynamic pressure was implemented to have adaptive microlenses for microfluidics network applications.[29] For the purpose of our current paper, we will address only EO tunable microlenses that utilize EO lanthanum-modified lead zirconate titanate (PLZT) ceramics.

A tunable EO PLZT microlens with annular electrode structure has been proposed previously.[30] This design, with its ring electrode structure, is simple to realize, relatively free of diffraction effects, and allows for the maximum possible fill factor. It is worth noting that the microlens realized with ring electrodes can be operated in a mode that is polarization independent.[30]

The organization of the paper is as follows. In Sec. 2, we discuss in detail the numerical modeling of our proposed lenslet structure leading to calculation of the focal length and its dependence on applied voltage. In Sec. 3, we show the essential simulation results of a z-scan of such a linear electro-optic lens, which can be used to determine the focal length. Section 4 summarizes the fabrication method for such lenses. Last, in Sec. 5, we provide the experimental

---

[*]Current address: American Science and Technology Corporation, 815 Medary Avenue, Suite 118, Brookings, SD 57006.

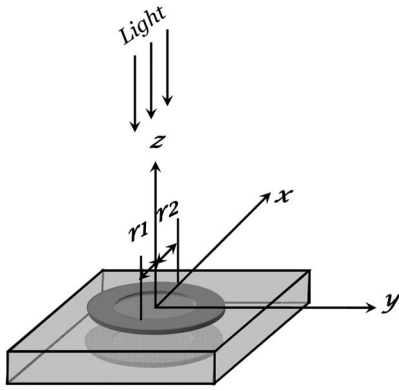**Fig. 1** An illustration of a concentric electrode PLZT microlens adapted from Ref. 28.
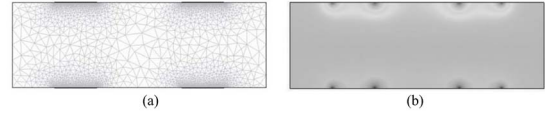

Fig. 2 (a) The adaptive mesh generation using COMSOL (FEM-LAB), and (b) the surface plot of an induced electrostatic potential due to an applied voltage of 180 V. Note the mesh size variation at the electrode regions due to adaptive meshing.

results of the focal length as derived from a z-scan and compare these with the numerical results developed in Sec. 2.

2 Numerical Modeling of Adaptive Micro-Lens: Focal Length Dependence on Applied Voltage

We have chosen the annular electrode design[30] illustrated in Fig. 1 for modeling purposes. In previous work, the electrostatic potential was found by numerically solving the Laplacian equation, where the surface charge method[31] was incorporated. The refractive index distribution within the lens aperture and the effective light path modulation was found by numerical integration over the entire substrate thickness. In this paper, finite element analysis (FEA) will be utilized to model the electrostatic field distribution within the lens aperture. Consequently, the net phase delay and the change of refractive index at each point within the substrate can be calculated, and hence the focal length can be determined.

2.1 Electro-optic Effect

PLZT is a polycrystalline EO material that has many advantages over single-crystal EO materials such as lithium niobate, including ease of fabrication, low operating voltages, and reduced long-range strain effects. It also has advantages over ferroelectric liquid crystals due to its solid phase nature and fast switching speeds.[32] In the absence of an applied field, the PLZT is optically isotropic. An applied electric field induces refractive index anisotropy. This leads to an optical phase difference φ for the two orthogonally polarized light components passing through the material. The relative phase change, i.e., the EO response, is assumed to be quadratic, that is, $\varphi \propto E^2$, where E is the amplitude of the applied electric field. The transmission intensity I of the light through the EO system is given by:[32]

$$I = \frac{1}{2}\sin^2\left(\frac{\varphi}{2}\right), \tag{1}$$

where φ is the phase change incurred during travel through the material. The relative change in the phase $\Delta\varphi$ due the applied voltage is:[32]

$$\Delta\varphi = k_o \Delta n L, \tag{2}$$

where $k_o = 2\pi/\lambda_o$, L is the PLZT wafer thickness, λ_o is the incident light wavelength, and Δn is the change of the refractive index birefringence due to the applied voltage. The induced ordinary and extraordinary index of refraction is determined by:

$$n_o = n_0 - \frac{1}{2}n_0^3 r_{12}, \quad n_e = n_0 - \frac{1}{2}n_0^3 r_{11}, \tag{3}$$

where r_{11}, r_{12} are the quadratic EO coefficients. Hence,

$$\Delta n = n_o - n_e = \frac{1}{2}n^3 r_{eff} E^2, \quad r_{eff} = r_{21} - r_{11}. \tag{4}$$

2.2 Finite Element Simulation

Previously, the electrostatic potential within the PLZT material, for the concentric electrode design, was found by solving the Laplacian equation. This is not a trivial task, since we end up with a solution in the form of an integral equation that must be solved numerically.[30] This is a lengthy process, especially if we need to post-process the results to obtain information about lens performance. Furthermore, extending the method to address a lenslet array may require extensive algorithm developments.

Finite element analysis (FEA) is a powerful tool that has been implemented in many fields to model complicated physical problems.[33] As detailed elsewhere,[34] the accuracy of the solution depends on the mesh size. Smaller mesh sizes are needed for smaller structures to accurately account for the physical changes, while much larger structures can be handled nicely with coarser mesh sizes. This makes the FEA method a very powerful tool for modeling our lens structure. To illustrate this point, we demonstrate in Fig. 2(a) the cross section of a micro lens slab with substrate thickness of 500 μm and electrode thickness of 1 μm. The FE mesh was generated by COMSOL (FEMLAB) Multiphysics tools. Note the mesh density and element size variation around the electrode regions. The surface plot of the electrostatic potential due to 150-V applications is shown in Fig. 2(b).

COMSOL Multiphysics is a multiphysics software package where coupled thermal, mechanical, and electrostatic effects and chemical reactions, among other physical phenomena, can be studied concurrently.[33] This allows not only for studying the phase change due to the applied electric field, but also for studying reliability issues. In addition, optical materials' nonlinearity, scattering, and depolarization effects may be added for accurate modeling. Further-
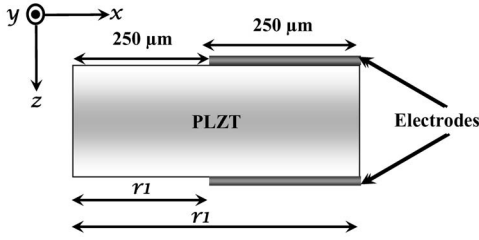
Fig. 3 Cross-sectional slice of the PLZT microlens structure under test. Note that the cross section is along the *x-z* direction and represents one-half of the lens structure. If we revolve this cross section around the *z* axis, we will obtain a cylinder where the lens aperture is in the middle, with inner and outer radii of r_1, r_2.

more, it is seamlessly interfaced with MATLAB, which allows for easier data post-processing by using the data in other subroutines, as we will show later.

2.3 Problem Definition

The first item of simulation is to identify the domain within the microlens structure in which the electrostatic potential distribution must be identified. Referring to Fig. 1 and the description provided in Ref. 30, we have a circularly, i.e., axially, symmetric electrode design. This means that if we have a slice along the *x-z* plane, as illustrated in Fig. 3, we can revolve this cross section around the *z* axis, and we will obtain a cylinder where the lens aperture lays in the middle, with inner and outer radii of r_1, r_2. Thus, the horizontal axis for all plots is *r*, while the vertical axis is *z*. All problems' dimensions are indicated in Fig. 3. It is worth pointing out that we choose the lens aperture such that it matches the substrate thickness for generating the most-quadratic phase profile, and hence an aberration-free lens.[30]

The refractive index change in the *x*- and *y*-polarization directions, respectively, can be written as:[30]

$$\Delta n_1(r,z) = n_0 \left\{ 1 - \frac{n_0^2}{2} [r_{11} E_r^2(r,z) + r_{12} E_z^2(r,z)] \right\}, \qquad (5)$$

$$\Delta n_2(r,z) = n_0 \left\{ 1 - \frac{n_0^2 r_{12}}{2} [E_r^2(r,z) + E_z^2(r,z)] \right\}. \qquad (6)$$

We set $r_{11} = 2.42 \times 10^{-16}$ m^2/V^2 and $r_{12} = -1.94 \times 10^{-16}$ m^2/V^2 (Ref. 30) as the values for electro-optic coefficients. One final note: We considered electrode thickness to be negligible.

In Figs. 4(a) and 4(b) we show plots for the induced electrostatic field component in the *z* and *r* directions, respectively, due to 300 V, i.e., 0.6 KV/m^2, applications. These plots are in the *x-y* cross section of Fig. 3, each 100 μm in the *z* direction. The corresponding change in the refractive index Δn for the *x* and *y* polarization states is shown in Figs. 4(c) and 4(d), respectively. These plots also correspond to the *x-y* plane and were taken in 100 μm increments in the *z* direction.

2.4 Focal Length Estimation

Figures 4(c) and 4(d) illustrate the change of refractive index, due to the applied potential, in the radial direction, i.e., *x-y* plane, within the lenslet aperture at various *z* levels

perpendicular to the direction of light propagation. This means that we can divide the lens structure, in the *z* direction with cross section of *x-y*, into thin subsections. Each subsection can be considered a slab of thin film that has the same refractive index profile. Now, several approaches can be used to calculate the net phase delay due to optical beam propagation through the lens structure. First, we can integrate over the entire structure, assuming an incident beam with plane wavefronts. Second, and more accurately, we can use the beam propagation method (BPM).[35] However, even for tightly focused beams, i.e., 20 to 40 μm, the Rayleigh length will be larger than our samples' thickness, which is 500 μm. Hence, the net phase delay can be approximately calculated as:

$$\Delta\varphi = n_0 k_0 \sum_{i=1}^{n} \Delta z_i \Delta n_i, \qquad (7)$$

where $n_0 = 2.54$ is the refractive index of the PLZT at 0 V, $k_0 \approx 10^7$ m^{-1} is the free-space wave number, Δz is the layer thickness, and Δn is the refractive index profile within such a layer. All calculation will be based on the use of an HeNe laser at a wavelength of 633 nm. Since Δz will always be a fixed quantity, we can rewrite Eq. (7) as follows:

$$\Delta\varphi = n_0 k_0 \Delta z \sum_{i=1}^{n} \Delta n_i. \qquad (8)$$

Since the substrate thickness is 500 μm, we have taken $\Delta z = 5$ μm, 1 μm, 0.5 μm for 100, 500, and 1000 layers, respectively. In our calculations, we have found that no matter how many layers were used in the calculation, the net phase change will always be the same. Therefore, all of the following calculations were based on 500 layers.

Once $\Delta\varphi$ is computed, based on Eq. (8) as illustrated in Fig. 5(a), we fit data points to a quadratic profile, assuming minimum induced lens aberration. It was shown previously that that minimum aberration can be achieved with a lens aperture equal to the substrate thickness.[30] All simulation provided here is based on a 1:1 ratio between the wafer thickness and lens aperture width. The equation for data fitting is in the form:

$$\Delta\varphi = ar^2 + br + c. \qquad (9)$$

Since the optical field distribution immediately behind the lens is

$$E \propto \exp\left(\frac{jk_0 r^2}{2f}\right), \qquad (10)$$

one can use the quadratic coefficient of Eq. (9) and Eq. (10) such that

$$\Delta\varphi = \frac{n_0 k_0 r^2}{2f} = ar^2, \qquad (11)$$

and hence,

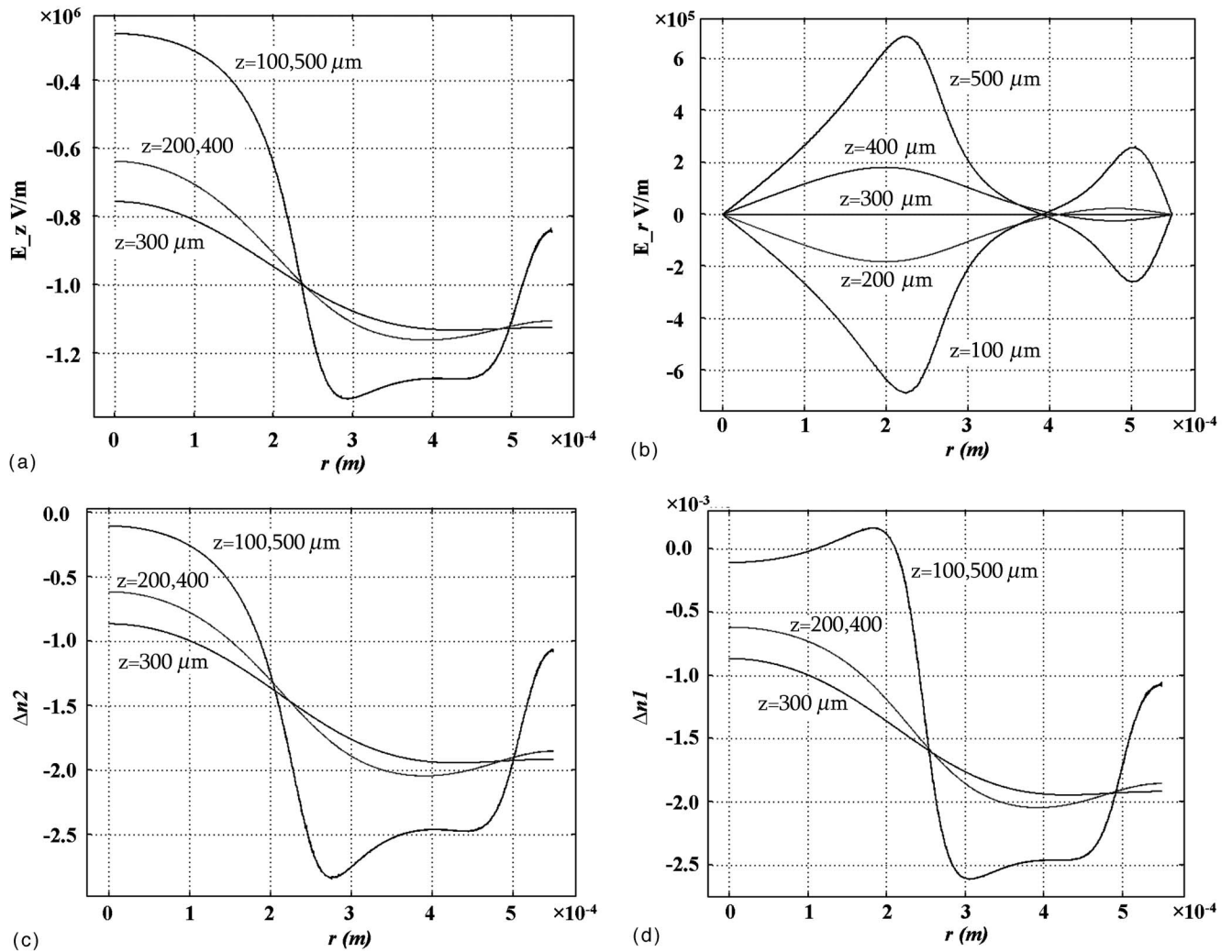$$f = \frac{k_0}{2an_0}. \qquad (12)$$

Fig. 4 (a) The induced electrostatic field in the *z* direction, (b) the induced electrostatic field in the *r* direction, (c) the radial variation of refractive index change for *x*-polarized light, and (d) the radial variation of the refractive index for *y*-polarized light. These results are for applied voltage of 300 V. Notice that the radial variation of the induced electrostatic field and refractive index change is in the *x*-*y* plane and at 100-μm increments in the *z* direction.

In Figs. 5(a) and 5(b), we illustrate the calculated net phase variation with the applied voltage and the corresponding focal length, respectively. Two major observations are noticed in Fig. 5(b). First, the induced lens is negative. Second, the focal length of the induced lens gets shorter as the applied voltage increases.

3 Microlens Characterization Using Z-Scan

The z-scan method is commonly used to determine the focal length of a nonlinearly induced lens. In this case, the lens under test is scanned along the propagation direction (*z*) around the back focal plane of an external lens that focuses a Gaussian beam onto the nonlinear sample. We employ the same method to determine the focal length for our microlenses, which can be regarded as a linear lens whose focal length, however, depends on the applied voltage. The characteristic signature of the z-scan of a linear lens is intrinsically different from that of a nonlinear induced lens. Details of the derivation of the z-scan graph for a linear lens along with a ray-optic verification of the wave

approach will be published elsewhere.[36] For our purposes, suffice to state that the experimental arrangement shown in Fig. 6 is used, where the output beam from a He-Ne laser is first expanded by a lens of focal length f_1 and then focused to a waist w_0 with a second lens of focal length f_2. The sample under test is scanned through a distance Δz about the location of this waist. The Gaussian optical field distribution at this plane, which is incident on the test lens of focal length f, can be expressed as:

$$E(x,y) = \frac{q_0}{q_0 + \Delta z} \exp\left[-\frac{j(x^2 + y^2)k_0}{2(q_0 + \Delta z)} \right],\qquad(13)$$

where q_0 $(=jz_R=jk_ow_0^2/2)$ is the *q*-parameter of the beam at the focus of the second external lens, and z_R is the Rayleigh range. Hence, the optical field distribution on the observation plane a distance $Z \gg \Delta z > z_R$ from the waist location can be expressed as:
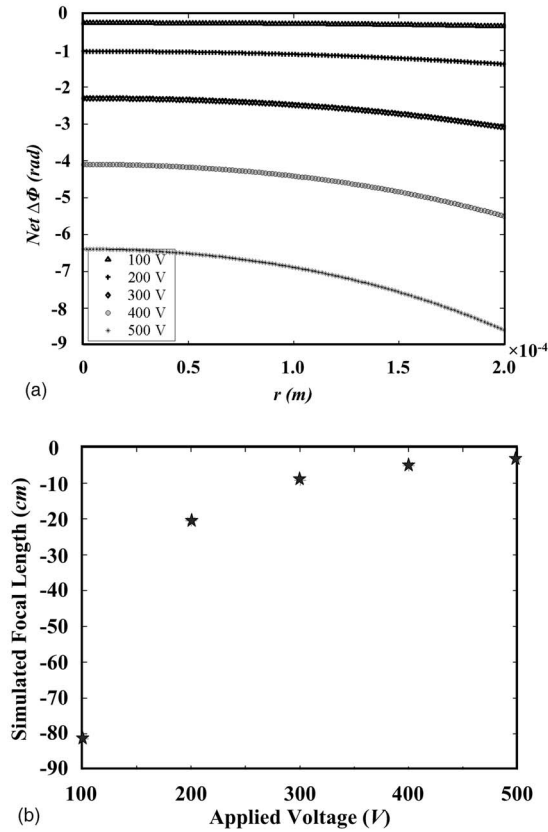
(a)

(b)

Fig. 5 (a) The induced net phase change as calculated using COM-SOL Multiphysics simulation results, and (b) the corresponding induced focal length variation as a function of the applied voltage. Notice that the induced focal length is negative, and hence we obtain a diverging lens, and that the net phase change increases with higher voltage values, and hence a shorter focal length is obtained. The preceding results are for the x polarization.

$$E(x,y,Z) = \frac{jk_0}{2\pi Z} \int \int \Im(x',y')$$
$$\times \exp\left\{-\frac{jk_0}{2Z}[(x-x')^2 + (y-y')^2]\right\} dx' dy',$$
$$\text{(14)}$$

where

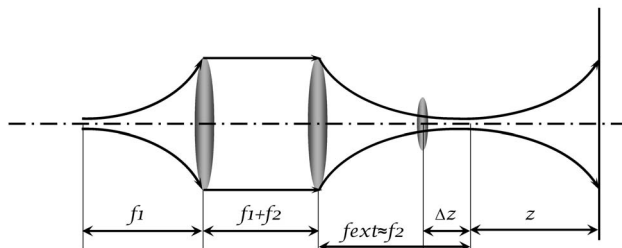$$\Im(x,y) = E(x,y)p_f(x,y)T_f(x,y). \quad \text{(15)}$$

Equation (15) has three terms:

- The Gaussian field distribution $E(x,y)$ given in Eq. (13),
- The aperture function:

$$p_f(x,y) = circ(r/r_0) = \begin{cases} 1 \rightarrow \text{for } r < r_0 \\ 0 \rightarrow \text{otherwise} \end{cases}, \quad \text{(16)}$$

- The lens transmission function:

$$T_f(x',y') = \exp\left[\frac{j(x^2+y^2)k_0}{2f}\right]. \quad \text{(17)}$$

The on-axis transmittance on the observation plane is given by:

$$I(0,0,Z) \propto E(0,0,Z)E^*(0,0,Z). \quad \text{(18)}$$

After considerable algebra, this can be expressed as:

$$I(0,0,Z) \propto \frac{k_0^2}{4\pi^2 Z^2 f^2} \frac{|q_0|^2}{|q_0|^2 + (\Delta z)^2} |q_z|^2$$
$$\times \left[1 + \exp\left(\frac{-k_0 r_0^2 b}{|q_z|^2}\right)\right.$$
$$\left. -2\exp\left(\frac{-k_0 r_0^2 b}{2|q_z|^2}\right)\cos\left(\frac{k_0 r_0^2 a}{2|q_z|^2}\right)\right], \quad \text{(19)}$$

where

$$\frac{1}{q_z} = \frac{1}{q_0 + \Delta z} + \frac{1}{Z} - \frac{1}{f}, \quad \text{(20)}$$

$$a = \text{Re}(q_z), \quad b = \text{Im}(q_z). \quad \text{(21)}$$

The first set of simulated data for normalized on-axis z-scan intensity, detected 1 m away from the focus of the test lens, was obtained for a probing beam of waist size 50 μm. For this beam waist size, the confocal parameter q_0 of the probing beam is $\approx$12.5 mm at HeNe laser wavelength λ=0.633 μm. In Fig. 7(a), we show typical z-scan plots for test lens focal length values that vary between 2 to 20 mm in 2-mm increments. Now, for a scanning distance $\Delta z = nz_0$, the beam radius $w(\Delta z = nz_0) \approx nw_0$. Accordingly, the test lens diameter was set to 1000 μm so that it is much larger than the probing beam width for the total scanning distance of $\Delta z = \pm 5z_0$. In Fig. 7(b), we assume a lens aperture of 250 μm (similar to that of our fabricated linear adaptive electro-optic lens) such that the probing beam size is comparable to the lens aperture at the end of the scanning distance. Hence, the on-axis Fresnel intensity is expected to show the diffraction effects from the lens edges. Notice that the intensity oscillations occur toward the end of the scanning distance.

Note that the maximum on-axis intensity is expected before the external focus for a negative lens and after the external focus for a positive lens. Around the external focus, the slope of the z-scan graph is negative for a negative focal length test lens and positive for a positive focal length test lens. The maximum on-axis intensity depends on the
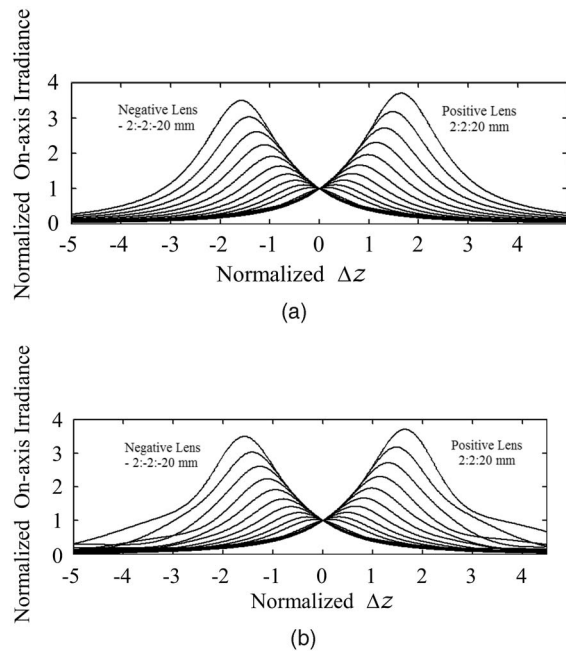

Fig. 6 A depiction of the focal length measurement experimental layout.

(a)

Fig. 7 Z-scan for linear lenses with focal length values that vary between ±2 to 20 mm in 2-mm increments: (a) without aperture diffraction, and (b) with aperture diffraction. Note that the maxima locations are independent of the diffraction effects. Furthermore, the diffraction affects the normalized irradiance amplitude toward the leading edge and the trailing edge of the positive and negative lenses, respectively.

magnitude of the focal length of the test lens. Also, note that the maxima locations are independent of the diffraction effects. Furthermore, the diffraction affects the normalized irradiance toward the leading edge and the trailing edges of the positive and negative test lenses, respectively. The z-scans of linear lenses are distinctively different from the z-scans of nonlinearly induced lenses, as in the conventional z-scan.[37] The rigorous wave approach can be reconciled with a simpler ray-optics picture; this is explained elsewhere.[36]

4 Device Fabrication

The starting material is a polycrystalline PLZT substrate, of composition 9/65/36. The processing steps of the electro-optic module are shown in Fig. 8. The fabrication has been performed at Case Western Microfabrication Laboratory. We start with a 4-in optically polished PLZT wafer. The objective of the process is to deposit the lens platinum (Pt) electrode structure according to our design. This electrode layer consists of two layers.

4.1 Wafer Cleaning

RCA [111] cleaning is a silicon standard cleaning process that consists of third steps. First, the wafer is degreased using acetone, methanol, and DI water rinse for 5 min each. This is usually followed by base and acid cleaning steps, each lasting for 20 min. Since acids, particularly sulphuric acid, may attack PLZT, one acid cleaning step is skipped. The composition of the base cleaning solution is ammonium hydroxide, hydrogen peroxide, and DI water with ra-
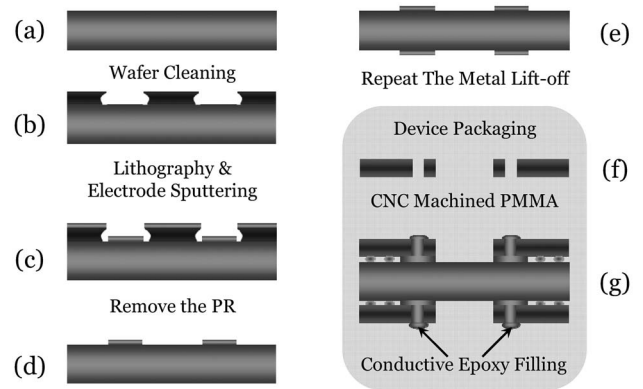

Fig. 8 The process flow steps for realizing the PLZT microlens array module. The major process steps include lift-off lithography to achieve the lenslet array and a packaging step.

tios of 1:1:5. This process is done for 15 min, followed by DI rinse for 5 min. The wafer is then dried with N_2.

4.2 Lift-Off Lithography

Prior to the lithography step, the wafer should be heated to 120 °C for 20 min to drive off any moisture and enhance the photoresist adhesion. The photolithography process for lift-off deposition can be summarized as follows:

1. Spin-coat Shipley AZ 1818 at 4000 rpm for 30 s.
2. Soft-bake for 20 to 30 min at 90 °C.
3. UV exposure for 12 s at 13 mW.
4. Soak the wafer in chloro-benzene for 90 s
5. Dry off the wafers with dry N_2.
6. Bake at 90 °C for 4 min to dry off any excess chloro-benzene.
7. Develop for 75 s in 4:1 positive developer and DI water.
8. Rinse the wafer in DI water for 5 min, and then blow dry.

4.3 Pt Deposition and Electrode Formation

Once the photolithography step is done, the wafer is ready for Pt electrode deposition. The Pt its to be sputtered using a 4-in target at 200-W radio frequency (RF) signal, 5-mTorr chamber pressure, and for 30 min. The desired Pt thickness is 3000 Å.

Once the deposition is complete, photoresist removal is done using a long soak in acetone. After, the wafer is cleaned with methanol and rinsed with DI water. Now, the device is ready for testing.

4.4 Device Packaging

Once we have realized the device structure, packaging is necessary. Plastic PMMA wafers of 1-mm thickness are used to package the PLZT to form an EO module. Using precision machining, the original mask information is fed to the program controlling the machine. Then vias, with sizes larger than the lenslet array outer electrode diameters, are etched precisely where the conducting contacts and other optical windows are needed, as shown in Fig. 8(f). The PLZT wafer is sandwiched between the two plastic
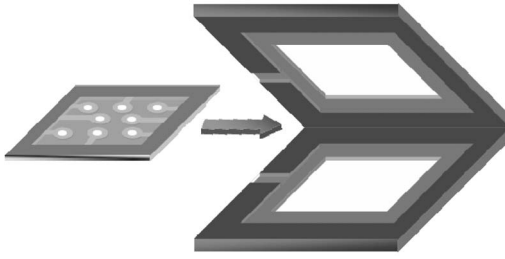
Fig. 9 A depiction of the final packaging process of the lenslet array module.

(a)

wafers, aligned to the vias, and then bonded to them with epoxy, as shown in Fig. 8(g). The vias are then filled with conductive polymer, and electrical contacts are made. The packaging process is illustrated in Fig. 9. The final results of the microlens array fabrication process and the packaged lens array module are shown in the optical micrographs of Figs. 10(a) and 10(b), respectively.

5 Experimental Determination of Focal Length and Discussion

Using the z-scan method developed earlier, one can determine the focal length of a linear lens. A typical experimental result for our adaptive electro-optic test lens with a bias voltage of 300 V is shown in Fig. 11(a), which suggests a focal length of approximately −10 cm. This value is then compared with our predictions from the numerical calculations using COMSOL tools, as shown in Fig. 5(b). The processed experimental results from the z-scan are compared with the simulated COMSOL results and are superposed in Fig. 11(b). Note that above 300 V, there is a good agreement between the COMSOL and the z-scan results, and the trend with increasing applied voltage for both cases is identical. The discrepancy between the two results for small values of the applied voltage may be due to the rather large and *negative* nonlinear optical refractive index coefficient $n_2 \approx -10^{-6}$ esu $\approx -10^{-12}$ m^2/W of PLZT thin films, as has been recently pointed out by Leng et al.,[38] which has not been included in our model for simplicity. We plan to investigate the combined effect of nonlinear and linear (external voltage induced) lensing in the future. We remark that scattering and depolarization effects,[32] and the piezoelectric effect[39] have also not been included in our model.
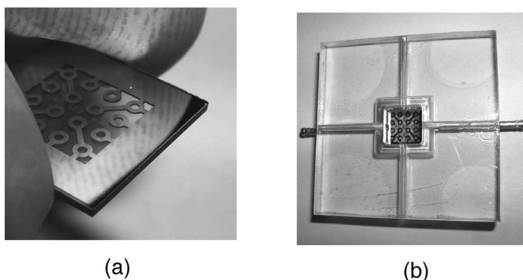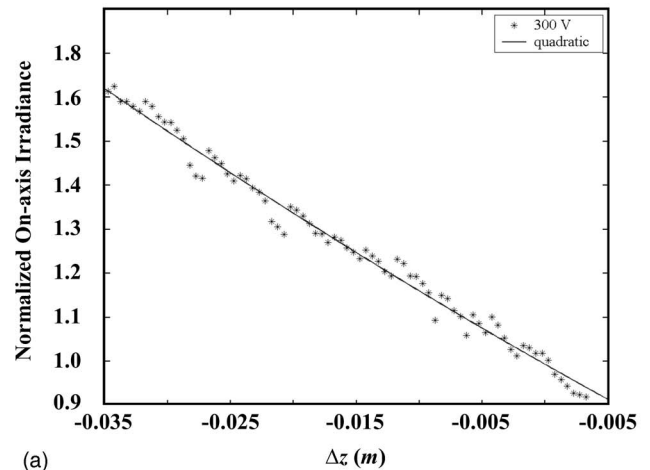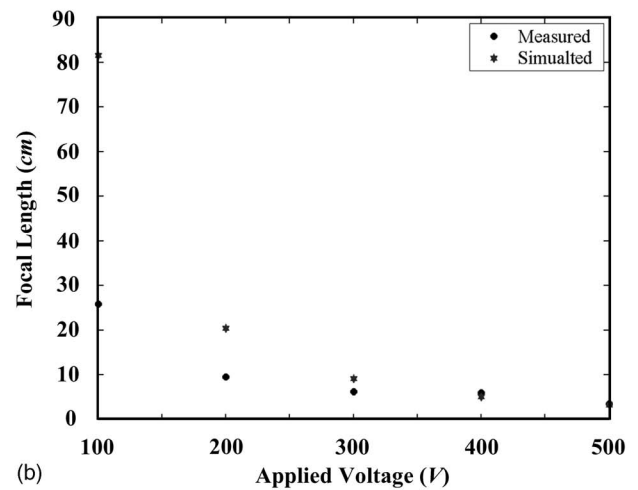

Fig. 11 A plot of the measured z-scan data for a 500-μm lens: (a) on-axis normalized irradiance plot at applied voltage of 300 V, and (b) comparison between the measured focal length and the simulated one obtained using COMSOL Multiphysics at various applied voltages.

(a) (b)

Fig. 10 The fabrication results of the PLZT micorlens array module: (a) 1-cm^2 die, and (b) the packaged lenslet array module.

References

1. W. B. Veldkamp, "Overview of micro-optics: past, present, and future," in *Miniature and Micro-Optics*, *Proc. SPIE* **1544** (1991).
2. K. Peterson, "Silicon as a mechanical material," *Proc. IEEE* **70**, 420–448 (1982).
3. I. B. Heard, R. Coquillé, D. Rivière, and P.-Y. Klimonda, "Characterization and reliability of a switch matrix based on MOEMS technology," *Microelectron. Reliab.* **43**, 1935–1937 (2003).
4. S. Sinzinger and J. Jahns, *Microoptics*, Wiley-VCH Verlag (1999).
5. Y. Huang, E. L. Mather, J. L. Bell, and M. Madou, "MEMS-based sample separation for molecular diagnostics," *J. Bioanal. Chem.* **372**, 49–65 (2002).
6. U. Staufer, T. Akiyama, C. Beuret, S. Gautsch, W. Noell, G. Schurmann, C. Stebler, and N. F. de Rooij, "Micro-electromechanical systems for nanoscience," *J. Nanopart. Res.* **2**, 413–418 (2000).
7. P. L. Gourley, "Biocavity laser for high-speed cell and tumor biology," *J. Phys. D* **36**, R228–R239 (2003).
8. J. A. Walker, "The future of MEMS in telecommunications network," *J. Micromech. Microeng.* **10**, R1–R7 (2000).

9. D. W. Monk and R. O. Gale, "The digital micromirror device for projection display," *Microelectron. Eng.* **27**, 489–493 (1995).
10. M. J. Feldstein, J. P. Golden, C. A. Rowe, B. D. MacCraith, and F. S. Ligler, "Array biosensor: Optical and fluidic system," *Biomed. Microdevices* **1:2**, 139–153 (1999).
11. A. E. Bruno, E. Baer, R. Völkel, and C. S. Effenhauser, "Microoptical fluorescence detection for chip-based multiplexed analysis systems," in *3rd International Conference on μ-TAS*, pp. 281–285 (1998).
12. V. Lehmann and S. Rönnebeck, "MEMS techniques applied to the fabrication of anti-scatter grids for x-ray imaging," *Sens. Actuators, A* **95**, 202–207 (2002).
13. P. Nussbaum, R. Vökel, H. P. Herzig, M. Eisner, and S. Haselbeck, "Design, fabrication and testing of microlens arrays for sensors and microsystems," *Pure Appl. Opt.* **6**, 617–636 (1997).
14. M. Davidson, "A microlens direct-write concept for lithography," in *Emerging Lithographic Technologies*, *Proc. SPIE* **3048**, 346–355 (1997).
15. N. Streibl, U. Nolscher, J. Jahns, and S. Walker, "Array generation with lenslet arrays," *Appl. Opt.* **30**, 2739–2742 (1991).
16. M. Kufner and S. Kufner, "Monolithically integrated refractive optical interconnection networks," in *Miniatures and Microoptics*, *Proc. SPIE* **1992**, 150–158 (1993).
17. R. Göring and S. Glöckner, "The potential of transmittive microoptical systems for miniaturized scanners, modulators and switches," *Miniaturized Systems and Microoptics*, *Proc. SPIE* **3008**, 70–81 (1997).
18. P. Savander and H-J. Haumann, "Microlens array used for collimation of linear laser diode array," *Meas. Sci. Technol.* **4**, 541–543 (1993).
19. S. Heinemann, "Computer generated beam shaping and focusing optical elements for laser materials processing," *Opt. Commun.* **119**, 613–622 (1995).
20. F. M. Dickey, "Laser beam shaping," *Opt. Photonics News* 30–35 (2003).
21. S. Heinemann, "Computer generated beam shaping and focusing optical elements for laser materials processing," *Opt. Commun.* **119**, 613–622 (1995).
22. W. W. Simmons, G. W. Leppelmeier, and B. C. Johnson, "Optical beam shaping using polarization effects," *Appl. Opt.* **13**, 1629–1632 (1997).
23. N. Streibl, U. Nölscher, J. Jahns, and S. Walker, "Array generation with lenslet array," *Appl. Opt.* **30**, 2739–2742 (1991).
24. Y. Abdelaziez and C. H. Ahn, "PLZT-based electro-optic modules for micromachined bio-photonics systems," *Proc. SPIE* **4561**, 171–182 (2001).
25. L. G. Commander, S. E. Day, and D. R. Selviah, "Variable focal length microlenses," *Opt. Commun.* **177**, 157–170 (2000).
26. H. Ren, Y.-H. Fan, and S.-T. Wu, "Polymer network liquid crystal for tunable microlens arrays," *J. Appl. Phys., J. Phys. D* **37**, 400–403 (2004).
27. K. T. Gahagan, V. Gopalan, J. M. Robinson, Q. X. Jia, T. E. Mitchell, M. J. Kawas, T. E. Schlesinger, and D. D. Stancil, "Integrated electro-optic lens/scanner in LiTaO$_3$ single crystal," *Appl. Opt.* **28**, 1186–1190 (1999).
28. B. Bergea and J. Peseux, "Variable focal lens controlled by an external voltage: an application of electrowetting," *Eur. Phys. J. E* **3**, 159–163 (2000).
29. N. Chronis, G. L. Liu, K.-H. Jeong, and L. P. Lee, "Tunable liquid-filled microlens array integrated with microfluidic network," *Opt. Express* **11**, 2370–2378 (2003).
30. M. Kulishov, "Adjustable electro-optic microlens with two concentric ring electrodes," *Opt. Lett.* **23**, 1936–1938 (1998).
31. M. A. Title and S. H. Lee, "Modeling and characterization of embedded electrode performance in transverse electrooptic modulator," *Appl. Opt.* **29**, 85–98 (1990).
32. P. E. Shames, P.-C. Sun, and Y. Fainman, "Modeling of scattering and depolarization electro-optic devices. 1. Characterization of lanthanum-modified lead zirconate titanate," *Appl. Opt.* **37**, 3717–3725 (1998).
33. *FEMLAB Technical Computing* magazine.
34. A. Sheffer and A. Ungör, "Efficient adaptive meshing of parametric models," in *ACM Symposium on Solid Modeling and Applications*, pp. 59–70 (2001).
35. T.-C. Poon and P. P. Banerjee, Chapter 2 in *Contemporary Optical Image Processing with MATLAB*, Elsevier Science (2001).
36. P. P. Banerjee and Y. Abdelaziez, "Z-scan of linear lenses," in preparation.
37. M. Sheik Bahae, A. A. Said, and E. W. Van Stryland, "High sensitivity single beam n$_2$ measurement," *Opt. Lett.* **14**, 955–957 (1989).
38. W. Leng, C. Yang, H. Ji, J. Zhang, J. Tang, H. Chen, and L. Gao, "Linear and nonlinear optical properties of (Pb,La)(Zr,Ti)O$_3$ ferroelectric thin films grown by radio-frequency magnetron sputtering," *J. Phys. D* **40**, 1206–1210 (2007).
39. A. Levstik, V. Bonnar, Z. Kutnjak, and M. Kosec, "Fatigue and piezoelectric properties of lead lanthanum zirconate titanate ceramics," *J. Phys. D* **31**, 2894–2897 (1998).

Yasser A. Abdelaziez is currently a consultant in the areas of microtechnology and adaptive micro-optics. During his PhD work at the University of Dayton, he investigated adaptive beam-shaping techniques using acousto-optics and a electro-optic microlens array. He was a postdoctoral fellow at University of British Columbia, where he worked on the fabrication and modeling on microstructured surfaces for reflective displays applications. His previous work included CMOS-based bond degradation sensors, capillary electrophoresis, and optical switching. His areas of interest are MEMS-based multisensor platform system architecture, micropower generation and management, multiphysics modeling, and polysaccharide-protein interaction force measurements. He has authored and coauthored more than 13 refereed journal and conference papers in the areas of MEMS and adaptive micro-optics. He has contributed to 2 pending patents and 3 patent disclosures.

Partha P. Banerjee is a professor in the Electrical and Computer Engineering Department (ECE) and the Electro-Optics Program at the University of Dayton. He served as chair of ECE from 2000-2005. Prior to Dayton, he was a professor of electrical and computer engineering at the University of Alabama in Huntsville. His areas of interest are nonlinear optics, photorefractive materials, acousto-optics, and image processing. He has authored or coauthored over 100 refereed journal publications, over 100 conference papers, three textbooks, and several invited book chapters. He is the coauthor of the books *Principles of Applied Optics* (Irwin/McGraw Hill 1991), *Computational Methods in Electromagnetic and Optical Systems* (Dekker 2000), and *Contemporary Optical Image Processing with MATLAB* (Elsevier 2001). He is a Fellow of the SPIE and the OSA, and is a senior member of the IEEE. He obtained the NSF Presidential Young Investigator Award in 1987.